Accepted Manuscript

Load Path Sensitivity and Fatigue Life Estimation of 30CrNiMo8HH

M. Noban, H. Jahed, E. Ibrahim, A. Ince

PII: S0142-1123(11)00286-6
DOI: 10.1016/j.ijfatigue.2011.10.009
Reference: JIJF 2755

To appear in: *International Journal of Fatigue*

Received Date: 4 May 2011
Revised Date: 24 October 2011
Accepted Date: 26 October 2011

Please cite this article as: Noban, M., Jahed, H., Ibrahim, E., Ince, A., Load Path Sensitivity and Fatigue Life Estimation of 30CrNiMo8HH, *International Journal of Fatigue* (2011), doi: 10.1016/j.ijfatigue.2011.10.009

Load Path Sensitivity and Fatigue Life Estimation of 30CrNiMo8HH

M. Noban, H. Jahed[1], E. Ibrahim, and A. Ince

Mechanical and Mechatronics Engineering Department

University of Waterloo

200 University Ave W, Waterloo, Ontario N2L 3G1, CANADA

Abstract

A set of strain-controlled biaxial proportional and non-proportional tests were conducted on solid and tubular specimens of 30CrNiMo8HH steel. The effect of the phase angle on fatigue life was studied. This effect becomes noticeable when applying a 90° out-of-phase loading, reducing the fatigue life by a factor up to 5. It has been shown that the material has no additional hardening due to out-of-phase loading. To account for this severe path dependency, a material dependent non-proportionality modification factor is proposed. This path dependent sensitivity factor is applied to six different fatigue parameters including maximum equivalent total strain, maximum equivalent stress, Smith-Watson-Topper, Fatemi-Socie, plastic strain energy density and total strain energy density to correlate the fatigue results. The predicted fatigue lives are compared with the experiments. The cyclic plasticity models of Mroz and Chaboche were successfully employed to model the cyclic behavior of 30CrNiMo8HH steel. It has been shown that estimations based on the proposed non-proportionality modification factor agree well with the experimental results.

Keywords: Sensitivity factor, Out-of-phase loading, Low cycle fatigue, Cyclic plasticity, Fatigue parameter.

1. Introduction

According to experiments on different materials, non-proportional loading is most often more damaging than proportional loading in low cycle fatigue region [1-3]. The reduction in fatigue life under non-proportional loading is attributed to the rotation of the maximum shear stress planes which initiates plastic deformation along several slip bands. The slip systems accompanying the non-proportional loading and their interactions are more than those with the proportional loading, resulting in more damaging effect. It is therefore worthwhile to take into account the loading path effect on the fatigue life prediction. In order to quantify the loading path effect on fatigue lives, several non-proportionality factors have been developed.

Kanazawa et al. [4] studied the behavior of 1% Cr-Mo-V under non-proportional loading. Explaining the difference in cyclic deformation behavior under non-proportional loading, they proposed a rotation factor that can be used for expressing the non-proportionality of the loading path. This factor is based on the shear strain range on the critical plane. Benallal and Marquis [5] introduced an instantaneous non-proportionality plastic variable useful for simulating the plastic behavior of materials under non-proportional loading. The prediction of this model for austenitic stainless steel type 316 under non-proportional loading agreed with the experimental results. McDowell et al. [6] developed a non-proportionality factor introduced in the plastic strain space. This model consisted of two coefficients:

[1] Corresponding author, Tel: +15198884567 x37826, email: hjahedmo@uwaterloo.ca

hardening coefficient and path dependent coefficient. Applying their model on type 304 stainless steel, they concluded that the additional hardening can be related to the limit stress surface rather than the yield surface. In 1995, Itoh et al. [7] used the same 304 stainless steel to define a non-proportionality factor based on the strain path. Their factor did not require any knowledge of the experimental cyclic stresses. They used the modified non-proportional strain obtained from this factor along with a material constant to correlate the non-proportional fatigue data within a factor of two scatter band. Later, Chen et al. [1] proposed a non-proportionality factor represented geometrically by the ratio of two areas defined by the loading path: the area of a circle with a radius equals to the maximum shear strain, and the swept area of the maximum shear strain in polar coordinate system. To calculate these two areas in one cycle, the variations in shear and normal strains for arbitrary directions of a material element were calculated and their maximum values in each direction are plotted in polar coordinate graphs to relate the angle to the maximum shear strain, resulting in an area enclosed by the curve. This area always lied inside a circle whose radius is equal to the maximum value of the shear strain reached in the whole cycle. The longest chord [8] and the minimum circumscribed ellipse [9] are the two other well-known approaches for defining non-proportionality factors in strain space. The former defines the amplitude of the shear stress as half the length of the longest chord between two points in the shear stress path, whereas the latter determines the shear stress amplitude from the root mean square of the major and minor axes of the minimum circumscribed ellipse. Tanaka [10] proposed a non-proportionality parameter as a function of normalized plastic increment. This parameter was applied to Chaboche plasticity model [11] and showed a good agreement with experimental results obtained under different loading paths. Tanaka's non-proportionality parameter was employed and further developed by other authors [12, 13]. Shamsaei et al [13] used the non-proportionality factor proposed by Tanaka with a simplified form of Armstrong-Frederick model [14] and evaluated the capability of their model in different non-proportional loading conditions.

The experimental work in this study was on chrome-nickel based material under multiaxial proportional and non-proportional loading. Several studies on this material have been reported in the literature. Vetter et al. [15] reported a set of fatigue experiments on a thick-walled plain and cross-bored pipes made from high alloy chrome-nickel steels under pulsating internal pressure. They showed that the improvement in the admissible pulsating pressure is not always achievable by the heat treatment to higher strength materials. Lagoda and Macha [16, 17] calculated the fatigue life of a chrome-nickel steel alloy under stress-controlled loading based on three different criteria of multiaxial fatigue. They employed Palmgren-Miner hypothesis [18] to calculate fatigue under random loading conditions. It was shown that the maximum shear and normal stresses on the fracture plane resulting from modifying the shear stress give the most realistic prediction of fatigue life. The influence of multiaxial loading on the fatigue life of chrome-nickel based materials was studied by Hug and Zenner [19]. They showed that the change in fatigue life under non-proportional loading depends on the non-proportional hardening effect, material and the experimental procedure. In 2000, Potter et al. [20] investigated the fatigue life of 30CrNiMo8 steel under combined bending and torsion for notched specimens. They used an integral approach in order to take into account the non-proportional loading effect on fatigue resistance. Later, Ahmadi and Zenner [21] represented a model to simulate the damage progress based on the growth of microcracks under the influence of cyclic loading for several steel alloys including 30CrNiMo8. Reasonable prediction accuracy was obtained for constant and variable amplitude loading cases.

In this paper, the results of a set of biaxial proportional and non-proportional strain-controlled tests on 30CrNiMo8HH steel were reported. Experimental results of in-phase and 90° out-of-phase loading were used to characterize and model the fatigue behavior of the material under different loading paths. Cyclic plasticity models of Mroz and Chaboche were employed to model the plasticity behavior of the material. It has been shown that proportional and 90° out-of-phase loads can be considered as the upper and lower fatigue life limits, respectively. A non-proportionality sensitivity factor suitable for this alloy was developed based on these limits. Using the proposed non-proportional sensitivity factor and the cyclic behavior as predicted by the prominent fatigue models, the fatigue life was estimated and compared to experimental life. It is shown that the predictions using the proposed factor works very well over a wide range of fatigue models.

2. Material and Testing

Tests were performed on 30CrNiMo8HH steel, chemical composition given in Table 1, with yield strength of 870 MPa. Cyclic axial and biaxial tests were performed based on ASTM-E606 and ASTM-E2207, respectively. Solid-bar specimens were used for tensile and cyclic axial tests, while thin-walled tubular specimens were used for pure torsion and biaxial tests. For strain-controlled tests, axial-torsion extensometer type 3550 was used. The gage length of the extensometer is 10 mm, and the full range is ± 0.5 mm in the axial direction and ± 3° in shear direction. All tests were performed at standard laboratory temperature and humidity using an Instron-8874 servo hydraulic tension-torsion machine. A complete characterization of this material under cyclic loading is given in [22].

More than 30 tests with different loading paths and strain amplitudes within low cycle fatigue regime were performed in order to obtain the fatigue properties of 30CrNiMo8HH. Fig. 1 shows the proportional and non-proportional loading paths included in this study. A summary of applied strain amplitudes and observed fatigue lives is shown in Table 2.

Table 1: Chemical composition of 30CrNiMo8HH

	C	Cr	Ni	Mo	Si	Mn	P	S	Fe
wt%	0.26-0.33	1.8-2.2	1.8-2.2	0.3-0.5	< 0.4	< 0.6	< 0.035	< 0.035	Balance

Fig. 1: Applied loading paths

Table 2: Experimental results

Load Path	Axial strain amplitude (mm/mm)	Shear strain amplitude (radians)	Strain Ratio ($\lambda=\gamma_a/\varepsilon_a$)	Observed Life
Tension	0.0071	0	0	1221
Tension	0.0072	0	0	1649
Tension	0.0046	0	0	3064
Tension	0.0051	0	0	2191
Tension	0.0040	0	0	12732
Tension	0.0034	0	0	25686
Tension	0.0042	0	0	11484
Tension	0.0100	0	0	500
Torsion	0	0.0106	∞	1414
Torsion	0	0.0106	∞	1833
Torsion	0	0.0106	∞	2341
Torsion	0	0.0079	∞	5200
Torsion	0	0.0080	∞	5500
Torsion	0	0.0139	∞	793
Torsion	0	0.0138	∞	1100
Torsion	0	0.0069	∞	13748
In-phase	0.0035	0.0065	1.87	3903
In-phase	0.0042	0.0096	2.26	1885
In-phase	0.0035	0.0065	1.87	4493
In-phase	0.0037	0.0083	2.27	2699
30 out of phase	0.0035	0.0067	1.90	1346
30 out of phase	0.0035	0.0066	1.88	2240
30 out of phase	0.0035	0.0070	2.01	1885
45 out of phase	0.0035	0.0068	1.96	1171
45 out of phase	0.0035	0.0066	1.91	1645
45 out of phase	0.0025	0.0093	3.73	1762
60 out of phase	0.0035	0.0067	1.92	1425
60 out of phase	0.0035	0.0067	1.91	1414
60 out of phase	0.0014	0.0074	5.26	4558
90 out of phase	0.0036	0.0068	1.90	1384
90 out of phase	0.0035	0.0068	1.93	1264
90 out of phase	0.0031	0.0060	1.91	1777
90 out of phase	0.0029	0.0056	1.89	1932
Square	0.0035	0.0067	1.92	805
Square	0.0035	0.0067	1.92	1078
Square	0.0025	0.0056	2.22	2300
Two-square	0.0035	0.0068	1.93	1265
Two-square	0.0035	0.0067	1.93	1324
Butter fly	0.0035	0.0066	1.90	789
Butter fly	0.0035	0.0066	1.89	1472

3. Plasticity Modeling

In practice, fatigue life prediction requires an estimation of the cyclic elasto-plastic response of the material which is found through adoption of a cyclic plasticity model. To model the cyclic behavior of 30CrNiMo8HH steel, two prominent plasticity models were utilized in this study: the Mroz model [23] and the Chaboche model [11].

Mroz presented a multi-surface model to simulate the stress-strain curve of a material subjected to cyclic loading. Establishing the concept of field of plastic moduli, Mroz generalized the uniaxial stress-strain state to multiaxial state. Each field of the plastic moduli is defined by a stress surface similar to the yield surface. Once the stress point in the stress space reaches the stress surface, this surface is activated and used for plastic modulus calculations. The translation direction of the yield surfaces is given by a

vector joining the present state of the stress, S_{ij}, on the yield surface with the stress state, S^*_{ij}, on the next yield surface which means that the two surfaces have a common normal vector. Fig. 2 shows a geometrical representation of Mroz model.

Fig. 2: Geometrical representation of the Mroz hardening rule

The movement of the center of the yield surface is defined by

$$da^k_{ij} = d\eta[(R_{k+1} - R_k)n_{ij} + a^{k+1}_{ij} - a^k_{ij}] \qquad (1)$$

where R_k and R_{k+1} are the radii of the active stress surface and the next stress surface, respectively. a^k_{ij} and a^{k+1}_{ij} are the centers of the active stress surface and the next stress surface, respectively. n_{ij} is the normal vector to the yield surface, and $d\eta$ is a material constant that is determined by the consistency of the yield condition.

The second plasticity model used in this study is the Chaboche model [11]. The stress-strain hysteresis is modeled by introducing a nonlinear recovery term associated with the strain memory effect. Equation (2) represents the Chaboche model with N back stress term.

$$da^k_{ij} = \frac{2}{3} C_k d\varepsilon^p_{ij} - \gamma_k a^k_{ij} dp \qquad k = 1, .. N$$

$$da_{ij} = \sum_{k=1}^{N} da^k_{ij} \qquad (2)$$

$$dp = \sqrt{\frac{2}{3} d\varepsilon^p_{ij} : d\varepsilon^p_{ij}}$$

where $d\varepsilon^p_{ij}$, dp and da^k_{ij} are increments of the plastic strain tensor, the equivalent plastic strain increment and the k[th] term of the increment of the back stress. C_k and γ_k are material constants found from the material's cyclic stress-strain curve.

The material constants of Mroz and Chaboche models for the case studied here were determined using stabilized uniaxial hysteresis curve and are given in Table 3. Seven non-proportional strain-controlled tests with different loading paths were chosen, and the results of the experiments were compared with these two models.

Fig. 3 shows the uniaxial hysteresis curves at two distinct strain amplitudes as predicted by the two plasticity models and are compared to the experimental results. This figure shows that the 30CrNiMo8HH steel does not exhibit a strong non-Masing behavior, which means that the employed cyclic plasticity models are suitable for this material. These models were used to predict stress responses induced by a variety of strain amplitudes as shown in Table 4. The results of cyclic stress-strain behavior of selected loading paths as predicted by the two models are shown in Fig. 4 and are compared with experimental measurements. Each figure includes predicted axial stress – axial strain, predicted shear stress – shear

strain, and predicted axial stress – shear stress hysteresis loops at the stabilized cycle. The amplitudes of input strains are also included for each loading path.

Table 3: Parameters for Mroz and Chaboche models for 30CrNiMo8HH

Mroz model						Chaboche model (σ_y = 400 MPa)			
R_1	400 MPa	H_1	226475 MPa			C_1	137882 MPa	γ_1	3457.9
R_2	502.7 MPa	H_2	8032 MPa			C_2	137189 MPa	γ_2	7027
R_3	601.8 MPa	H_3	34415 MPa			C_3	129281 MPa	γ_3	619.7
R_4	697.4 MPa	H_4	12229 MPa			C_4	136501 MPa	γ_4	4937.9
R_5	750 MPa	H_5	10000 MPa			C_5	10071 MPa	γ_5	0

Fig. 3: Comparing uniaxial cyclic stress-strain curve from experiments, Mroz, and Chaboche

Fig. 4: Comparing predicted hysteresis stress-strain loop with experimental data (sinusoidal waves)

Fig. 5: Comparing predicted hysteresis stress-strain loop with experimental data (other waves)

The uniaxial hysteresis predicted by Mroz model for 30CrNiMo8HH has an excellent agreement with the experimental results, and Chaboche model's prediction is also very good. However, Mroz model prediction in non-proportional loading shows a slight additional hardening (e.g., Fig. 5 a), this is not the case in Chaboche model prediction. During proportional loading, the directions of the deviatoric stress, back stress, normal vector and their increments are the same and hence the hardening rules play no role in the direction of the yield surface movement. In this kind of loading paths, the equivalent stress-strain curves predicted by different hardening rules follow the same trend of the uniaxial curve. However, under non-proportional loading, hardening rules have a major effect on the predicted stress-strain response of the material. Depending on the employed hardening rule, the center of the yield surface follows different paths in the stress space which results in different stress-strain response for a given loading path. Therefore, the multiaxial equivalent stress-strain curve can be different from that of uniaxial depending on the employed hardening rule. It can be demonstrated that the angle between the increment of back-stress and normal vector during non-proportional loading has a significant effect on the response of the hardening rule. This has previously been shown in the literature. Jiang and Sehitoglu [24] and Kurath [25] reported that multi-surface hardening models produce an extra non-proportional hardening under out-of-phase loading. They showed that this unwanted additional hardening depends on the employed hardening rule, and the number of stress surfaces of the multi-surface models. The results obtained in the current paper confirm this well-established fact. For materials with slight additional hardening (around 15%) such as 1%CrMoV, it has been shown that the stress predicted by multi-surface models under out-of-phase loading is good [26]. Also, nonlinear kinematic models predict no considerable extra hardening under out-of-phase loading [4, 27], which agrees with the results of the current study. A comparison between the two predictions of the employed plasticity models suggests that Chaboche model has a better agreement with the experimental results of 30CrNiMo8HH steel.

Experiments carried out under non-proportional loading did not show any signs of cyclic additional hardening for 30CrNiMo8HH steel, as shown in Fig. 6. However, there is a considerable life reduction of 30CrNiMo8HH under non-proportional loading. This agrees with other observation concerning other material with no additional hardening [28]. For example, quenched and tempered 1050 steel with no additional hardening exhibit larger drop in fatigue strength under out-of-phase loading, as compared with 304L stainless steel with 55% non-proportional hardening coefficient [28, 29]. During non-proportional loading, more slip planes will be activated as compared to the proportional loading [30]. However, this does not necessarily mean that additional hardening always occurs under non-proportional loading; it happens due to the interaction of slip planes on one another at different directions [31-33]. In fact, the interaction of the slip systems is more important than their numbers [33]. Moreover, the additional hardening is highly dependent on the microphysical characteristics of the material [31, 34]. From microstructural point of view, a material exhibits additional hardening when dislocations in different directions delay the movement of other slip mechanism. In this kind of materials, the movement of the dislocations decreases during non-proportional loading and hence it is expected that the material will show more additional hardening, such as Zircaloy-4 [35] and SS304 [36]. In general, the value of additional hardening not only dependent on the material [32], but it also depends on a combination of material in an alloy [34], loading path [4] and temperature of the alloy [37]. Thus, before performing a non-proportional test, it is difficult to estimate quantitatively the value of additional hardening.

The cause of lower lives in non-proportional loading is not necessarily the additional hardening, rather it depends on the sensitivity of material to out-of-phase loading that additional hardening may be one part of it. Here we propose a material dependent sensitivity factor to take care of the load path and the phase angle.

Fig. 6: Multiaxial cyclic behavior of 30CrNiMo8HH under proportional and non-proportional loading

4. Fatigue Life Prediction

Six different fatigue damage parameters of maximum equivalent strain, maximum equivalent stress, Smith-Watson-Topper, Fatemi-Socie, plastic strain energy density and total strain energy density have been considered here to correlate the fatigue results.

4.1. Maximum equivalent strain parameter

Maximum equivalent strain, which uses von Mises equivalent strain, is widely used as damage parameter in the literature [1, 38, 39]. Generally, von Mises equivalent plastic strain is defined as

$$\varepsilon_{eq}^{p} = \sqrt{\frac{2}{3}\varepsilon_{ij}^{p} : \varepsilon_{ij}^{p}} \tag{3}$$

When applying a tension-torsion loading on a specimen and assuming incompressible plane stress condition, equivalent plastic strain can be written in the form

$$\varepsilon_{eq}^{p} = \sqrt{\varepsilon_{p}^{2} + \frac{\gamma_{p}^{2}}{3}} \tag{4}$$

where ε_p and γ_p are the axial and shear plastic strains associated with the directions of loading, respectively.

Equivalent strain ε_{eq} can be defined similar to the equivalent plastic strain [1, 39]

$$\varepsilon_{eq} = \sqrt{\varepsilon^2 + \frac{\gamma^2}{3}} \tag{5}$$

where ε and γ are the total axial and shear strain, respectively. Equivalent Poisson's ratio is taken to be 0.5.

4.2. Maximum equivalent stress parameter

Another fatigue parameter is von Mises equivalent stress [40]. Von Mises equivalent stress in deviatoric stress space is defined as

$$\sigma_{eq} = \sqrt{\frac{3}{2} S_{ij} : S_{ij}} \tag{6}$$

where S_{ij} are the components of deviatoric stresses.

In the special case of biaxial tension-torsion loading, Eq. (6) may be written in the form

$$\sigma_{eq} = \sqrt{\sigma^2 + 3\tau^2} \tag{7}$$

where σ and τ are the axial and shear stresses, respectively.

4.3. Smith, Watson and Topper (SWT) parameter

In 1970, Smith et al. [41] proposed the SWT parameter, $D_{p_{SWT}}$, which is based on the principal strain range and the maximum stress on the plane of the principal strain range. They argued that this parameter can be used for both proportional and non-proportional loading and also can account for the mean stress effect. This model can be written in the form

$$D_{p_{SWT}} = \sigma_{n,max} \frac{\Delta\varepsilon_1}{2} \tag{8}$$

where $\Delta\varepsilon_1$ is the principal strain range. $\sigma_{n,max}$ is the maximum stress on the principal strain range plane.

4.4. Fatemi-Socie parameter

Fatemi and Socie parameter [42] is a parameter defined according to the critical plane approaches. This parameter is obtained by the normal stress on the maximum shear strain plane as shown in the following form

$$D_{p_{FS}} = \gamma_{max}\left(1 + \frac{k\sigma_n^{max}}{\sigma_y}\right) \tag{9}$$

where γ_{max} is the maximum shear strain. σ_n^{max} is the maximum normal stress on γ_{max} plane. k is a constant obtained by fitting the uniaxial data against the pure torsion data. Assuming the constant $k = 1$, Fatemi-Socie parameter has been applied on the material considered in this study.

4.5. Plastic strain energy density parameter

Energy approach [43, 44] is considered as one of the most useful models for multiaxial loading since it considers both stress and strain components in the fatigue calculations. The plastic strain energy density per cycle may be regarded as a composite measurement of the amount of fatigue damage per cycle, so that the fatigue resistance of a metal may be characterized in terms of its capacity to absorb and dissipate plastic strain energy density [3]. For general multiaxial loading, the plastic work for a cycle can be calculated from

$$\Delta W_c^p = \oint_{cycle} \sigma_{ij} d\varepsilon_{ij}^p \tag{10}$$

where σ_{ij} and ε_{ij}^p are the stress and the plastic strain components, respectively. Increment of the total strain can be divided into the plastic and elastic strain increments parts

$$d\varepsilon_{ij}^t = d\varepsilon_{ij}^p + d\varepsilon_{ij}^e \tag{11}$$

Multiplying the stress tensor by the above equation and integrating over a full cycle results in

$$\oint \sigma_{ij} d\varepsilon_{ij}^t = \oint \sigma_{ij} d\varepsilon_{ij}^p + \oint \sigma_{ij} d\varepsilon_{ij}^e \tag{12}$$

For the set of biaxial tests included in this study the elastic work over the closed cycle is zeros, hence the second part of the right side of Eq. (12) is equal to zero, making the total cyclic energy equal to the cyclic plastic energy. Therefore, the cyclic plastic energy in tension-torsion can be defined as

$$W_p = \oint \sigma_{ij} d\varepsilon_{ij}^t = \oint \sigma d\varepsilon + \oint \tau d\gamma \tag{13}$$

4.6. Total strain energy density parameter

This parameter consists of cyclic plastic and positive elastic energy density as a parameter for predicting the fatigue life. This parameter allows consideration of mean stress. The total cyclic strain energy using [45] can be expressed as

$$W_t = W_p + W_e^+ \tag{14}$$

W_p and W_e^+ are the cyclic plastic and the positive elastic energy. W_e^+ is expressed as

$$W_e^+ = \oint < \sigma_{ij} >< d\varepsilon_{ij}^e >$$
$$< x >= x, \quad x \geq 0$$
$$< x >= 0, \quad x < 0 \tag{15}$$

5. Non-proportionality Factor

In the cyclic tests performed on 30CrNiMo8 it was observed that 90° out-of-phase loading is the most damaging loading path among all other non-proportional paths. On the other hand, the proportional loading tests had the highest fatigue life. Accordingly, the 90° out-of-phase loading is taken as the lower limit of the fatigue life, whereas the in-phase loading is taken as the upper fatigue life limit. All other loading paths are generally fitting in between these two limits. In reviewing the correlation of the fatigue data with different fatigue parameter in section 4, in all cases, there was a scatter in non-proportional results. This shows that loading path needs to be incorporated in the damage parameter. A method for such consideration is discussed below.

Assume a fatigue damage model in the following form

$$D = f(N_f) \tag{16}$$

where D is a fatigue damage parameter, which can be one of the six parameters considered here or any other parameter, and N_f is the fatigue life. For proportional loading in low cycle fatigue region, consider a power law function relationship between the fatigue life, N_{fP}, and the damage parameter,

$$D = m(N_{fP})^n \tag{17}$$

where m and n are material constants.

Various non-proportionality factors have been proposed to quantify the effect of the loading path on the fatigue life predictions. In this paper, the method of minimum circumscribed ellipse [9] is employed to determine the non-proportionality factor. The following path dependent non-proportional parameter in low cycle fatigue is considered here,

$$D_{NP} = D(1 + \alpha\psi) = f(N_{fNP}) \tag{18}$$

where D_{NP} is the non-proportional damage parameter modified by the factor $(1 + \alpha\psi)$, where ψ is the non-proportionality factor which depends on the strain path; and α is introduced as a non-proportional sensitivity material constant. Accordingly, fatigue life under non-proportional loading can be determined from the following equation

$$N_{fNP} = f^{-1}(D_{NP}) = f^{-1}[D(1 + \alpha\psi)] \tag{19}$$

The non-proportionality factor, ψ, is determined from the ratio of the minor axis, *b*, to the major axis, *a,* of the minimum circumscribed ellipse defined by the strain path, as illustrated in Fig. 7. In this figure, determination of, ψ, is given for a general non-proportional case, and for the special cases of 0° and 90° out-of-phase.

Fig. 7: Non-proportionality factor, , for three different loading paths

The non-proportionality sensitivity constant, α, depends on the change in the material behavior because of the rotation of principal axes in out-of-phase loading. For the quantification of this constant, the fatigue data for 90° out-of-phase loading is related to the in-phase fatigue data. Knowing the values of the

damage parameter, D, before modification, ψ for non-proportional loading and the values for m and n for the proportional loading, α can be determined using Least Square Method. It is worth mentioning that the constants m and n for the employed fatigue parameters including energy-based, strain-based and stress-based models are determined using the proportional fatigue data in low cycle fatigue regime, in which the plastic strain is dominant. Fig. 8 illustrates how the constant α is determined. The sensitivity parameter, α, is determined by minimizing the difference between the 90° out-of-phase fatigue curve and the proportional fatigue curve. Then, a single value of α is assumed for the rest of the non-proportional fatigue data.

Fig. 8: Determination of from the fatigue results of 90° out-of-phase loading and proportional loading

The proposed modification factor has been applied to the six fatigue life prediction models. To do this, first the value of ψ for all non-proportional loading paths considered in this study are obtained. Table 4 summarizes the calculated parameter ψ for some selected load paths. The fatigue parameters α, m and n are calculated for each fatigue model and are presented in Table 5.

Table 4: Non-proportionality factor, ψ, for different loading paths

Selected Load Paths	Axial strain amplitude (mm/mm)	Shear strain amplitude (radians)	Strain Ratio ($\lambda=\gamma_a/\varepsilon_a$)	Non-proportionality Factor ψ
Tension	0.0051	0	0	0
Tension	0.0100	0	0	0
Torsion	0	0.0081	∞	0
Torsion	0	0.0139	∞	0
In-phase	0.0042	0.0095	2.26	0
In-phase	0.0035	0.0064	1.87	0
90 out of phase	0.0036	0.0068	1.90	0.924
90 out of phase	0.0029	0.0056	1.93	0.924
45 out of phase	0.0025	0.0093	3.73	0.299
60 out of phase	0.0014	0.0075	5.26	0.277
Square	0.0025	0.0056	2.22	0.781
Two-square	0.0034	0.0067	1.93	0.544
Butter fly	0.0035	0.0066	1.89	0.703

Table 5: Material constants m, n and sensitivity factor for different fatigue models

Fatigue Model	Formulation	m	n	α
Strain approach D_p =Mmaximum equivalent strain	$D_p = m_\varepsilon N_f^{n_\varepsilon}$	0.128	-0.387	1.115
Stress approach D_p =Maximum equivalent stress	$D_p = m_\sigma N_f^{n_\sigma}$	1158.7	-0.072	0.150
Critical plane approach D_p =Fatemi-Socie model	$D_p = m_{FS} N_f^{n_{FS}}$	0.307	-0.427	0.761

Critical plane approach D_p =SWT model	$D_p = m_{SWT} N_f^{m_T}$	61.147	-0.369	1.320
Plastic energy approach D_p =cyclic plastic energy	$D_p = m_{PE} N_f^{m_E}$	2783.1	-0.779	1.284
Plastic and positive elastic energies D_p =plastic + positive elastic energy	$D_p = m_{TE} N_f^{m_T}$	1410.4	-0.674	0.816

Fig. 9-Fig. 14 compare the estimated and observed fatigue lives based on the six different approaches before and after applying the modification factor. The modified models show a closer agreement with the experimental results.

Fig. 9: Predicted fatigue life vs. experiments before, (a), and after, (b), applying loading path effect (Maximum equivalent strain)

Fig. 10: Predicted fatigue life vs. experiments before, (a), and after, (b), applying loading path effect (Maximum equivalent stress)

Fig. 11: Predicted fatigue life vs. experiments before, (a), and after, (b), applying loading path effect (SWT)

Fig. 12: Predicted fatigue life vs. experiments before, (a), and after, (b), applying loading path effect (Fatemi-Socie)

Fig. 13: Predicted fatigue life vs. experiments before, (a), and after, (b), applying loading path effect (Cyclic plastic energy)

Fig. 14: Predicted fatigue life vs. experiments before, (a), and after, (b), applying loading path effect (Total strain energy)

The figures on the left side, (a), show the fatigue lives predicted by the original fatigue damage models, while the figures on the right side, (b), show the prediction after applying the modification factor. Since the proposed non-proportionality factor does not affect the proportional loadings including tension and pure torsion loading; the fatigue life prediction for these tests are the same before and after applying the modification factor. However, the fatigue life prediction for non-proportional loading has considerably improved after applying the non-proportionality factor. Most of the modified non-proportional fatigue lives are within a factor of 2 scatter band.

6. Conclusion

A wide range of fatigue results for 30CrNiMo8HH are presented as the basis for evaluating and comparing six different fatigue parameters.

Two different plasticity models have been examined for simulating the cyclic behavior of 30CrNiMo8HH steel. While Mroz model successfully predicted the uniaxial hysteresis loops, Chaboche

model has a better agreement with the experimental results in modeling the response of material under multiaxial loading.

A non-proportional modification factor has been proposed to account for the sensitivity of the material to the non-proportional loading and its effect on fatigue life predictions. The proposed non-proportionality factor is dependent on the loading path and the fatigue damage parameter. This modification factor has been applied to six different fatigue damage parameters and used for predicting the fatigue life for non-proportional loading cases. The modified fatigue damage parameters correlate the predicted and experimental fatigue lives within a factor of 2 scatter band.

Based on the results presented, the following conclusions may be drawn from this study:

1- The fatigue life of 30CrNiMo8HH reduces by a factor of up to five when loading path changes from a simple proportional loading to 90^o out-of-phase loading.
2- Since the observed additional hardening in 90^o out-of-phase loading is not significant, the drop in fatigue life of 30CrNiMo8HH cannot be attributed to additional hardening, but rather related to a non-proportional sensitivity constant. During non-proportional loading, the number of planes experiencing high stresses is more than that in proportional loading. Therefore, more weak planes and defects will be involved in damage accumulation, which leads to higher probability of producing early cracks and hence lower fatigue life under non-proportional and out-of-phase loading.
3- To account for the loading path in fatigue life estimation, a two-fold modification factor is proposed. This modification factor takes the load history into account using the minimum circumferential ellipse method. Also, it provides a measure for the sensitivity of the material to the loading path. This measure is defined based on the 0^o and 90^o out-of-phase loadings, through difference minimization of the two paths.
4- The proposed modification factor shows very good estimation results when compared to a wide range of experimental results on 30CrNiMo8HH.
5- In general, the fatigue damage models which combine both stress and strain components give more realistic fatigue life predictions compared to the models that use only stress or only strain components.

Acknowledgements

The authors gratefully acknowledge the financial assistance of the Natural Sciences and Engineering Research Council (NSERC) of Canada.

References

[1] X. Chen, Q. Gao, X.F. Sun, Low-cycle fatigue under non-proportional loading, Fatigue & Fracture of Engineering Materials & Structures, 19 (1996) 839-854.
[2] X. Chen, Q. Gao, X.F. Sun, Damage analysis of low-cycle fatigue under non-proportional loading, International Journal of Fatigue, 16 (1994) 221-225.
[3] D. Socie, G. Marquis, Multiaxial fatigue, Society of Automotive Engineers, 2000.
[4] K. Kanazawa, K.J. Miller, M.W. Brown, Cyclic deformation of 1% cr-mo-v steel under out-of-phase loads, Fatigue & Fracture of Engineering Materials & Structures, 2 (1979) 217-228.
[5] A. Benallal, D. Marquis, Constitutive equations for nonproportional cyclic elasto-viscoplasticity, Journal of Engineering Materials and Technology, 109 (1987) 326-336.
[6] D.L. McDowell, An evaluation of recent developments in hardening and flow rules for rate-independent, nonproportional cyclic plasticity, Journal of Applied Mechanics, 54 (1987) 323-334.
[7] T. Itoh, M. Sakane, M. Ohnami, D.F. Socie, Nonproportional low cycle fatigue criterion for type 304 stainless steel, Journal of Engineering Materials and Technology, 117 (1995) 285-292.
[8] J. Lemaître, J. Chaboche, Mechanics of solid materials, Cambridge University Press, 1994.
[9] M.d. Freitas, B. Li, J.L. Santos, A numerical approach for high-cycle fatigue life prediction with multiaxial loading, in: S. Kalluri, P. Bonacuse (Eds.) Multiaxial fatigue and deformation: Testing and prediction, ASTM, 2000, pp. 139–156.
[10] E. Tanaka, A nonproportionality parameter and a cyclic viscoplastic constitutive model taking into account amplitude dependences and memory effects of isotropic hardening, European journal of mechanics. A. Solids, 13 (1994) 155-173.
[11] J.L. Chaboche, Time-independent constitutive theories for cyclic plasticity, International Journal of Plasticity, 2 (1986) 149-188.
[12] J. Zhang, Y. Jiang, Constitutive modeling of cyclic plasticity deformation of a pure polycrystalline copper, International Journal of Plasticity, 24 (2008) 1890-1915.
[13] N. Shamsaei, A. Fatemi, D.F. Socie, Multiaxial cyclic deformation and non-proportional hardening employing discriminating load paths, International Journal of Plasticity, 26 (2010) 1680-1701.
[14] P.J. Armstrong, C.O. Frederick, A mathematical representation of the multiaxial bauschinger effect, Technical Report RD/B/N/731, C.E.G.B., (1966).
[15] G. Vetter, D. Lambrecht, G. Mischorr, Fatigue of thick-walled pipes from soft martensitic and semi-austenitic chrome-nickel steels under pulsating internal pressure, Chemical Engineering & Technology, 15 (1992) 300-312.
[16] T. ŁAgoda, E. Macha, Estimated and experimental fatigue lives of 30crnimo8 steel under in-and out-of-phase combined bending and torsion with variable amplitudes, Fatigue & Fracture of Engineering Materials & Structures, 17 (1994) 1307-1318.
[17] T. Lagoda, E. Macha, Fatigue life estimation for 30crnimo8 steel under in- and out-of-phase combined bending and torsion with variable amplitudes, Materials Science, 31 (1996) 23-31.
[18] M.A. Miner, Cumulative damage in fatigue, J. Appl. Mech., 12 (1945) A159-A164.
[19] J. Hug, H. Zenner, Influence of multi-axial loading on the lifetime in lcf strength, in: K. Rie, P. Portella (Eds.) Low cycle fatigue and elasto-plastic behaviour of materials, Elsevier, 1998, pp. 217-222.
[20] K. Potter, F. Yousefi, H. Zenner, Experiences with lifetime prediction under multiaxial random loading, in: S. Kalluri, P. Bonacuse (Eds.) Multiaxial fatigue and deformation: Testing and prediction, ASTM, 2000, pp. 157–172.
[21] A. Ahmadi, H. Zenner, Lifetime simulation under multiaxial random loading with regard to the microcrack growth, International Journal of Fatigue, 28 (2006) 954-962.
[22] M. Noban, H. Jahed, S. Winkler, A. Ince, Fatigue characterization and modeling of 30crnimo8hh under multiaxial loading, Materials Science and Engineering: A, 528 (2011) 2484-2494.
[23] Z. Mróz, On the description of anisotropic workhardening, Journal of the Mechanics and Physics of Solids, 15 (1967) 163-175.

[24] Y. Jiang, H. Sehitoglu, Comments on the mroz multiple surface type plasticity models, International Journal of Solids and Structures, 33 (1996) 1053-1068.
[25] Y. Jiang, P. Kurath, A theoretical evaluation of plasticity hardening algorithms for nonproportional loadings, Acta Mechanica, 118 (1996) 213-234.
[26] (!!! INVALID CITATION !!!).
[27] Y. Jiang, P. Kurath, Characteristics of the armstrong-frederick type plasticity models, International Journal of Plasticity, 12 (1996) 387-415.
[28] N. Shamsaei, A. Fatemi, D.F. Socie, Multiaxial fatigue evaluation using discriminating strain paths, International Journal of Fatigue, 33 (2011) 597-609.
[29] N. Shamsaei, Multiaxial fatigue and deformation including non-proportional hardening and variable amplitude loading effects, in, University of Toledo, 2010.
[30] M. DL, P. RK, S. D, A. SD, Effects of nonproportional cyclic loading histories on type 304 stainless steel, in: Proceeding of the international spring meeting of societe Francaise de Metallurgie, Paris, 1984, pp. 53–86.
[31] S.H. Doong, D.F. Socie, Deformation mechanisms of metals under complex nonproportional cyclic loading, in: Proc., Third Int. Conf. on Biaxial/Multiaxial Fatigue, 1989.
[32] S.-H. Doong, D.F. Socie, I.M. Robertson, Dislocation substructures and nonproportional hardening, Journal of Engineering Materials and Technology, 112 (1990) 456-464.
[33] S. Calloch, D. Marquis, Additional hardening due to tension-torsion nonproportional loadings: Influence of the loading path shape, Multiaxial fatigue and deformation testing techniques, (1997) 113.
[34] M.V. Borodii, S.M. Shukaev, Additional cyclic strain hardening and its relation to material structure, mechanical characteristics, and lifetime, International Journal of Fatigue, 29 (2007) 1184-1191.
[35] X. Lin, Cyclic deformation behavior and dislocation substructures of hexagonal zircaloy-4 under out-of-phase loading, Journal of Engineering Materials and Technology, 122 (2000) 42-48.
[36] S. Kida, T. Itoh, M. Sakane, M. Ohnami, D.F. Socie, Dislocation structure and non-proportional hardening of type 304 stainless steel, Fatigue & Fracture of Engineering Materials & Structures, 20 (1997) 1375-1386.
[37] D. Bettge, W. Oesterle, J. Ziebs, Temperature dependence of additional cyclic hardening of a nickel-base superalloy during out-of-phase multiaxial deformation, Journal Name: Scripta Metallurgica et Materialia; Journal Volume: 32; Journal Issue: 10; Other Information: PBD: 15 May 1995, (1995) Medium: X; Size: pp. 1601-1606.
[38] B. Li, L. Reis, M. de Freitas, Simulation of cyclic stress/strain evolutions for multiaxial fatigue life prediction, International Journal of Fatigue, 28 451-458.
[39] V. Aubin, P. Quaegebeur, S. Degallaix, Cyclic behaviour of a duplex stainless steel under multiaxial loading: Experiments and modelling, in: M.d.F. Andrea Carpinteri, S. Andrea (Eds.) European structural integrity society, Elsevier, 2003, pp. 401-422.
[40] R.I. Stephens, A. Fatemi, R.R. Stephen, H.O. Fuchs, Metal fatigue in engineering, Second ed., John Wiley & Sons, Inc., 2001.
[41] K.N. Smith, P. Watson, T.H. Topper, A stress-strain function for the fatigue of metals, Journal of Materials, 5 (1970) 767-778.
[42] A. Fatemi, D.F. Socie, A critical plane approach to multiaxial fatigue damage including out-of-phase loading, Fatigue & Fracture of Engineering Materials & Structures, 11 (1988) 149-165.
[43] C.E. Feltner, J.D. Morrow, Microplastic strain hysteresis energy as a criterion for fatigue fracture, ASME J Basic Engng, 83 (1961) 15-22.
[44] Y.S. Garud, A new approach to the evaluation of fatigue under multiaxial loadings, Journal of Engineering Materials and Technology, 103 (1981) 118-125.
[45] F. Ellyin, D. Kujawshi, A multiaxial fatigue criterion including mean- stress effect, in: D.L. McDowell, R. Ellis (Eds.) Advances in multiaxial fatigue, ASTM STP, Philadelphia, 1993, pp. 55-66.

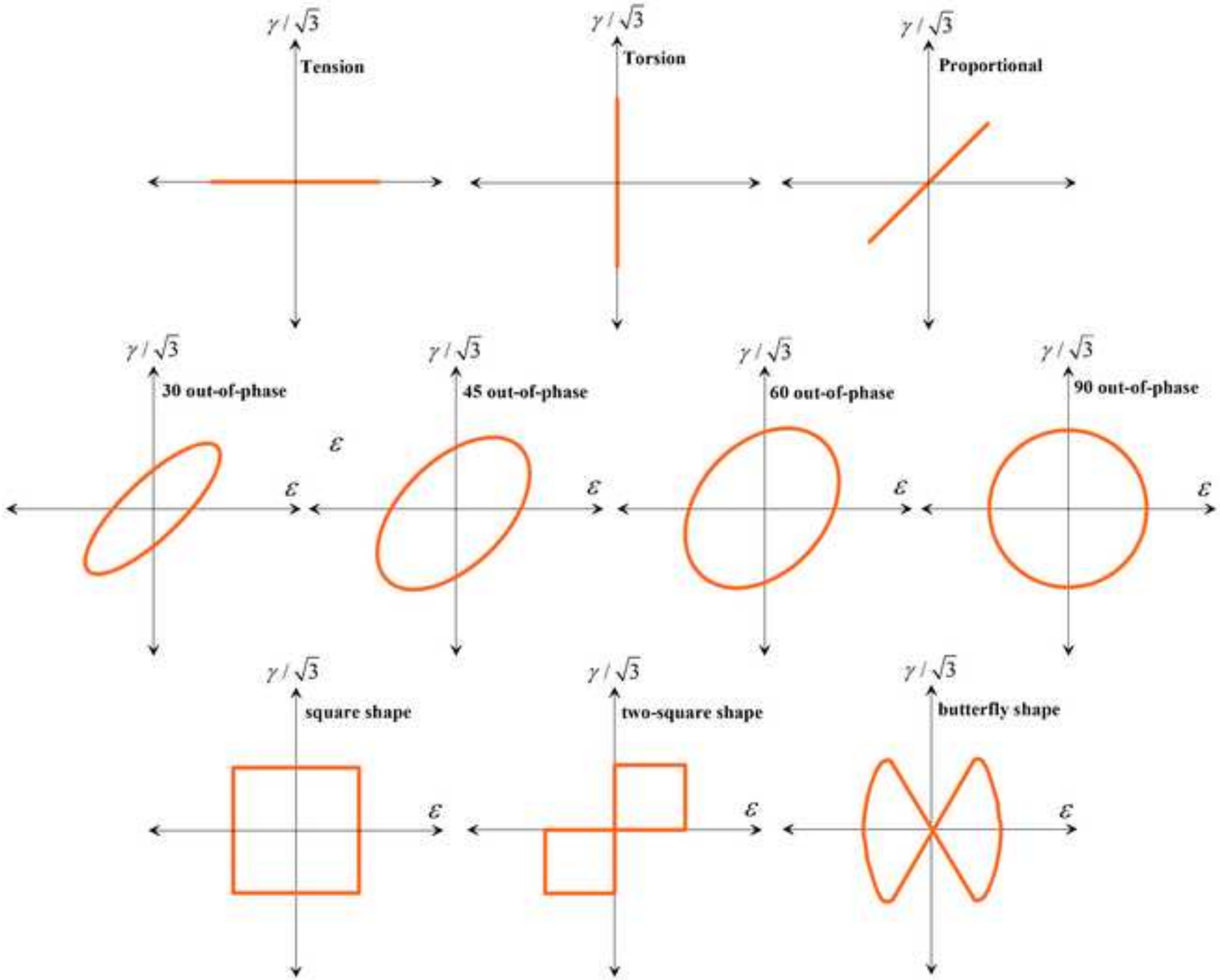

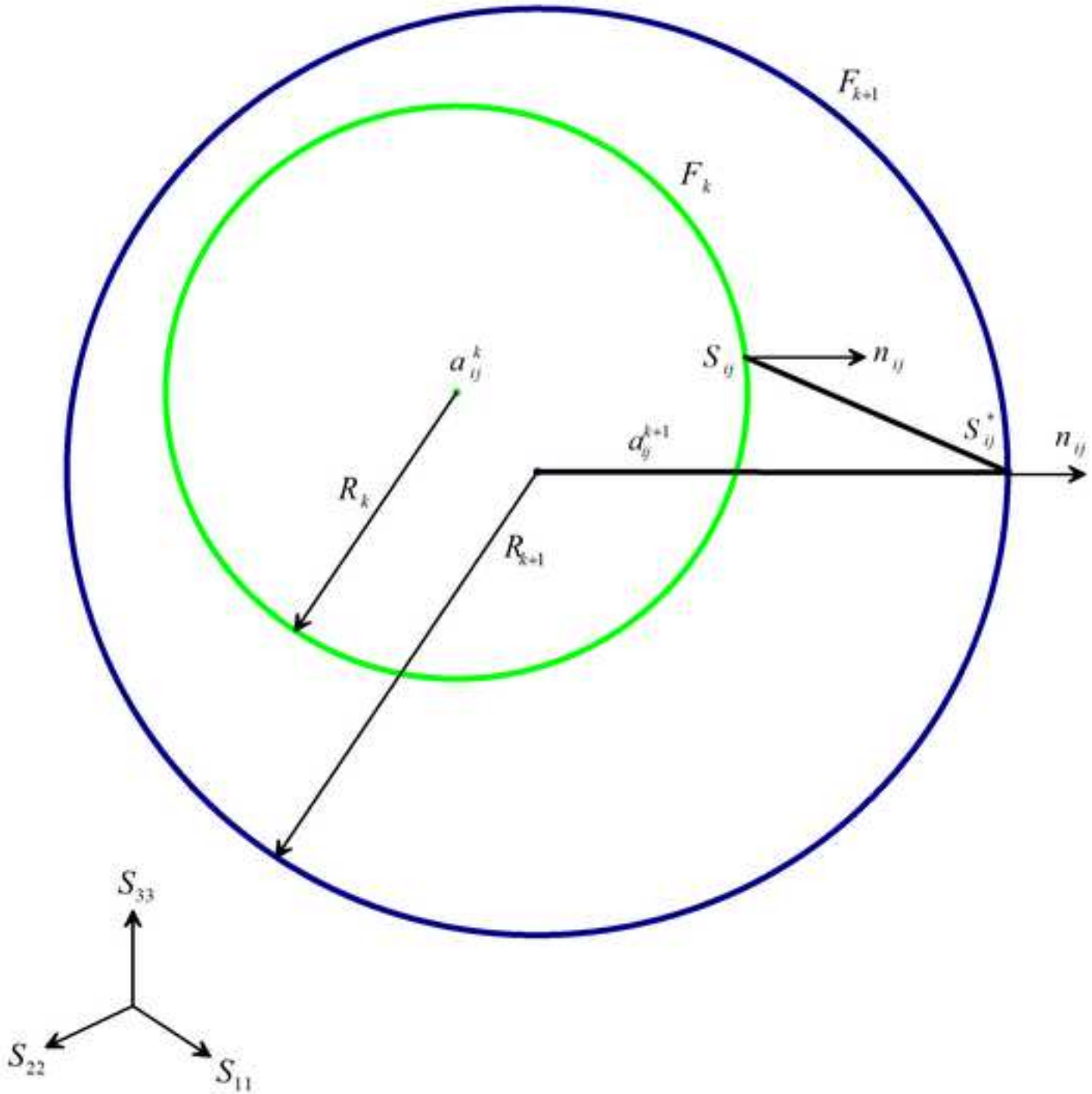

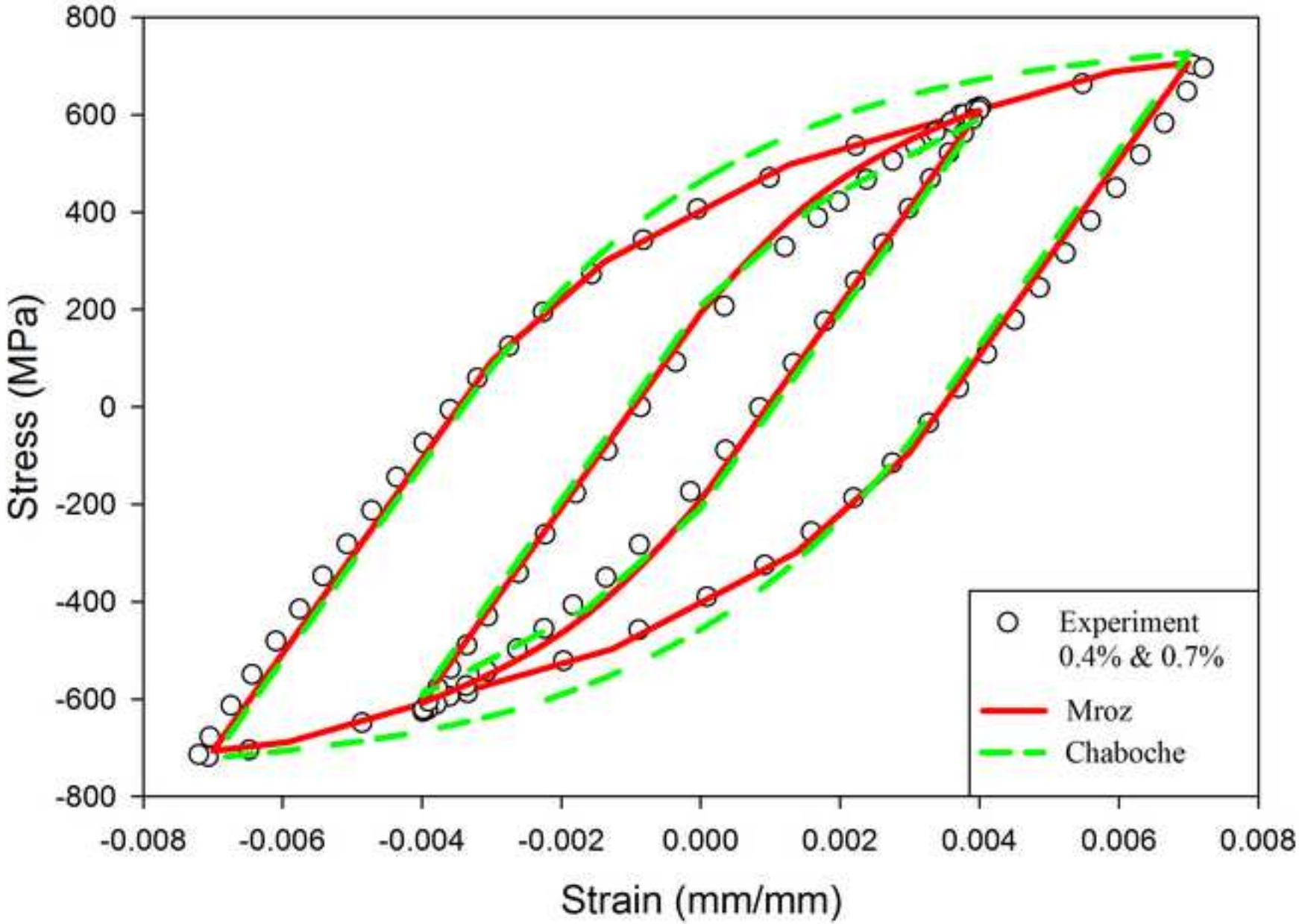

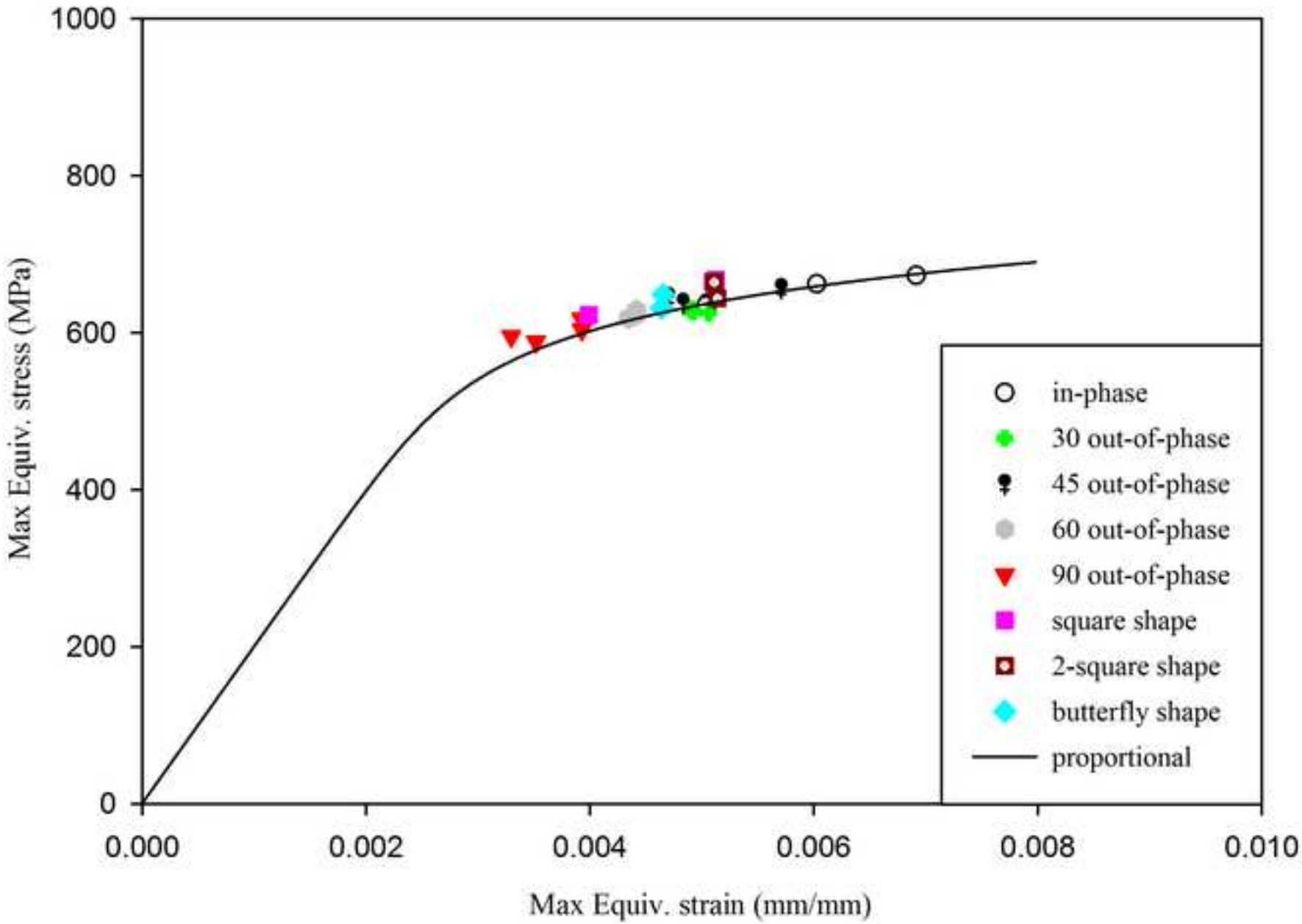

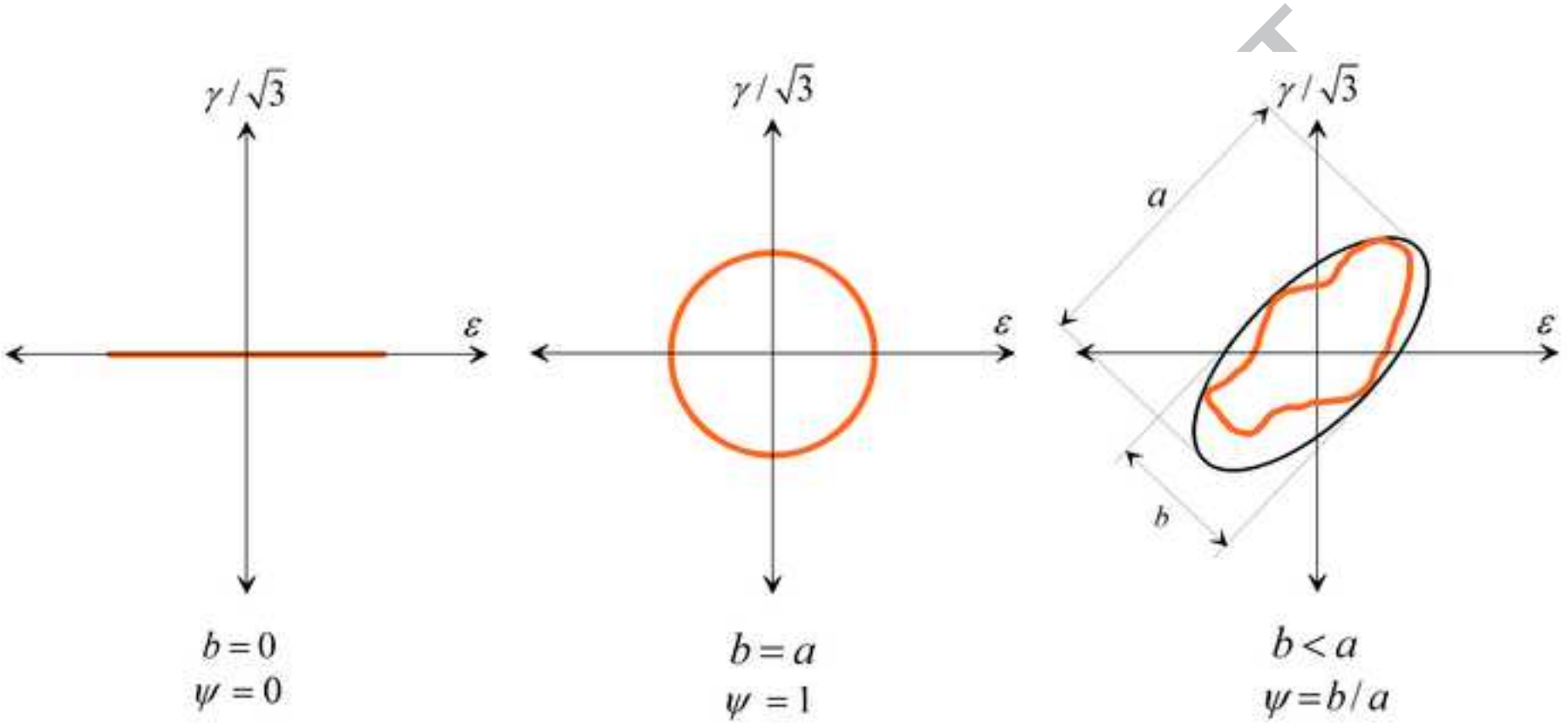

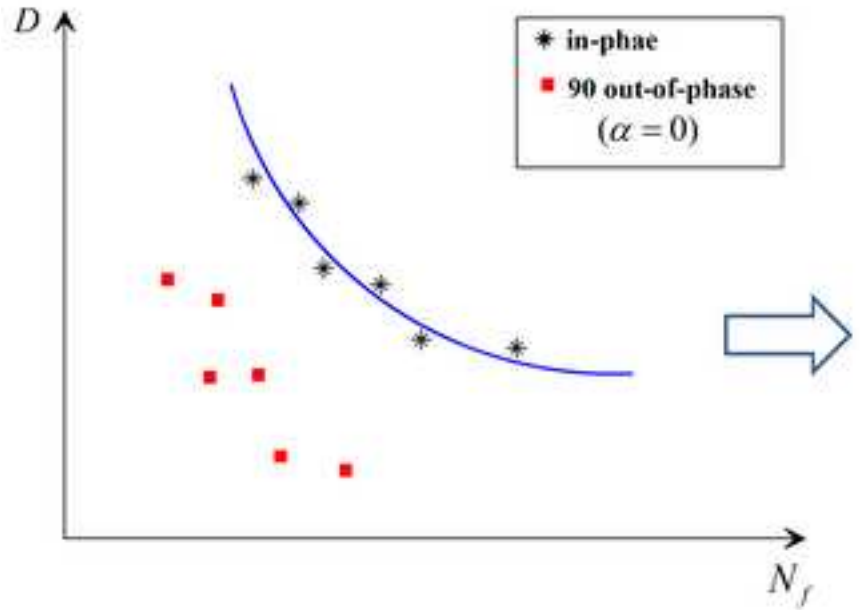

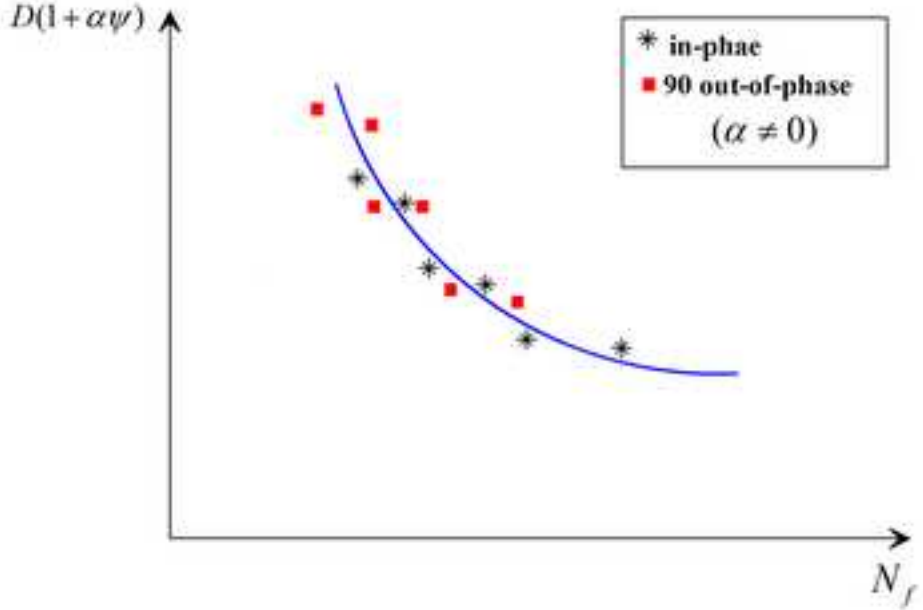

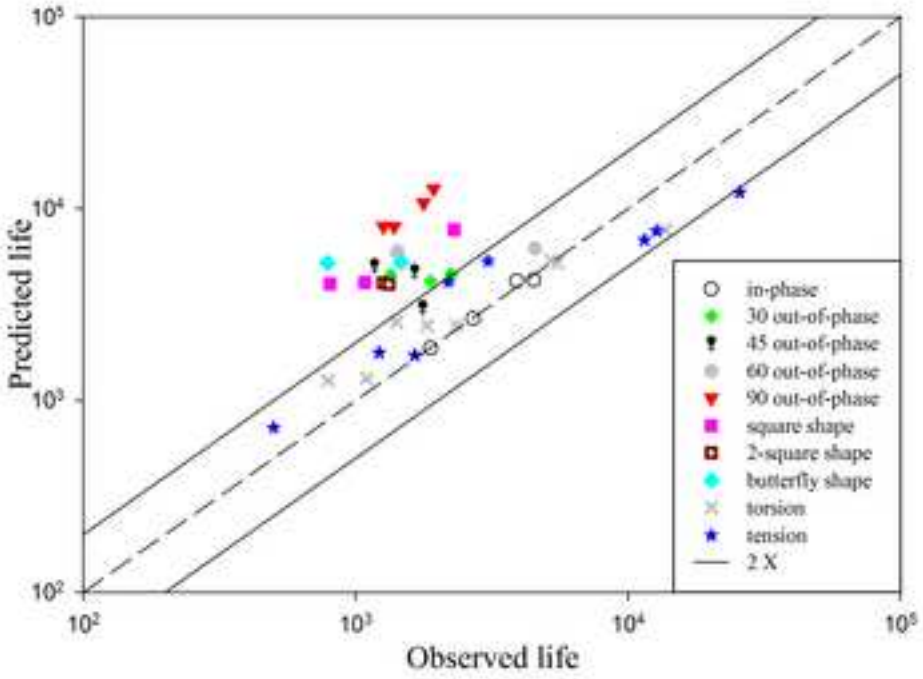

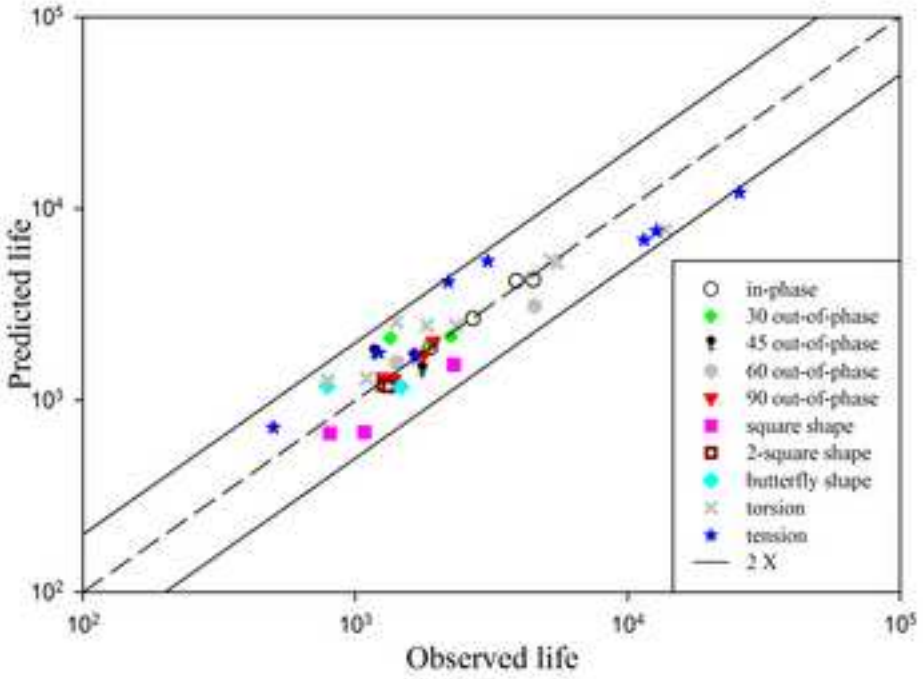

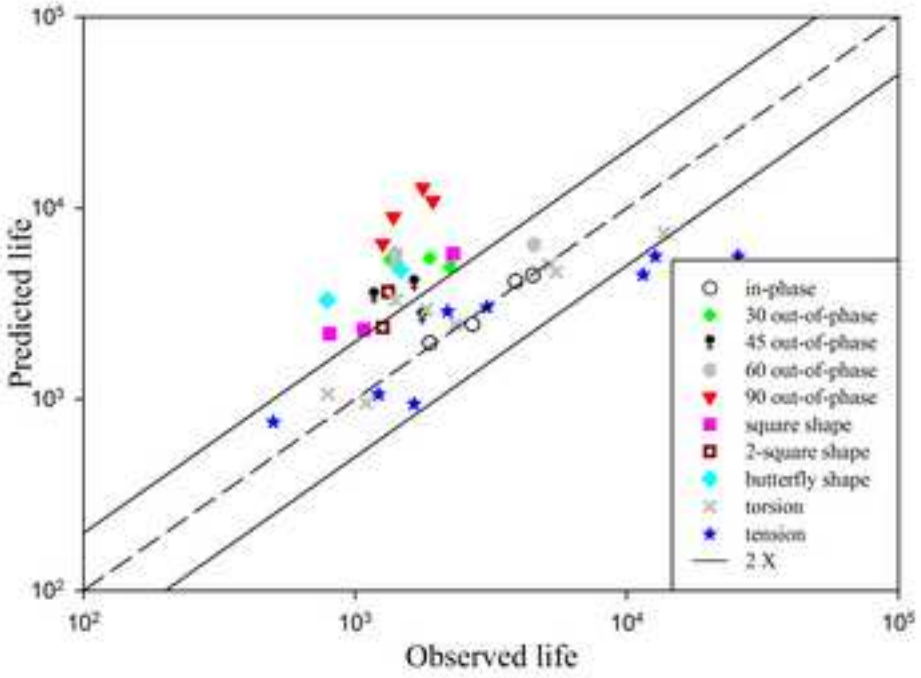

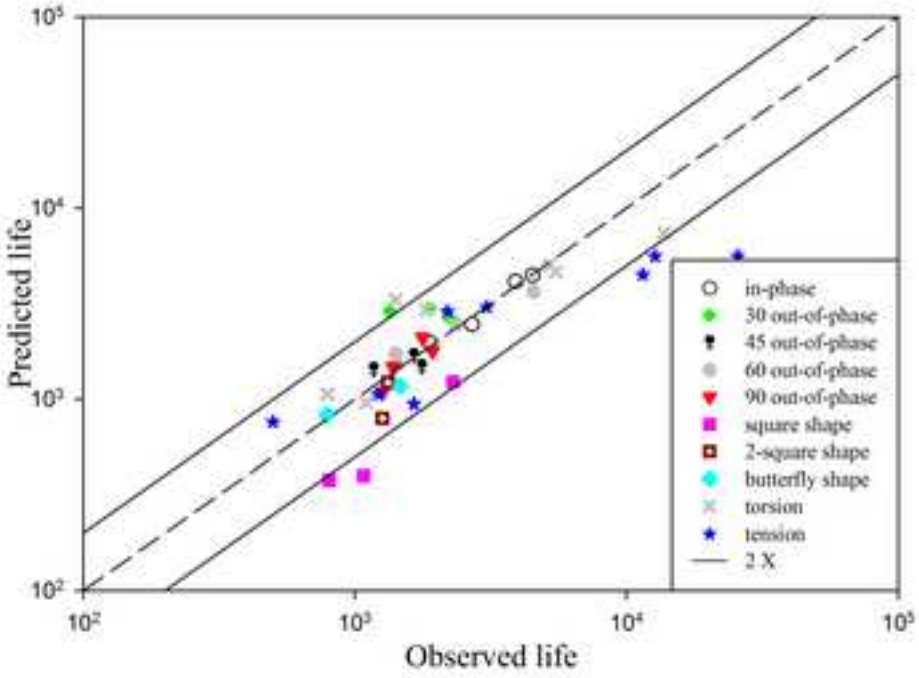

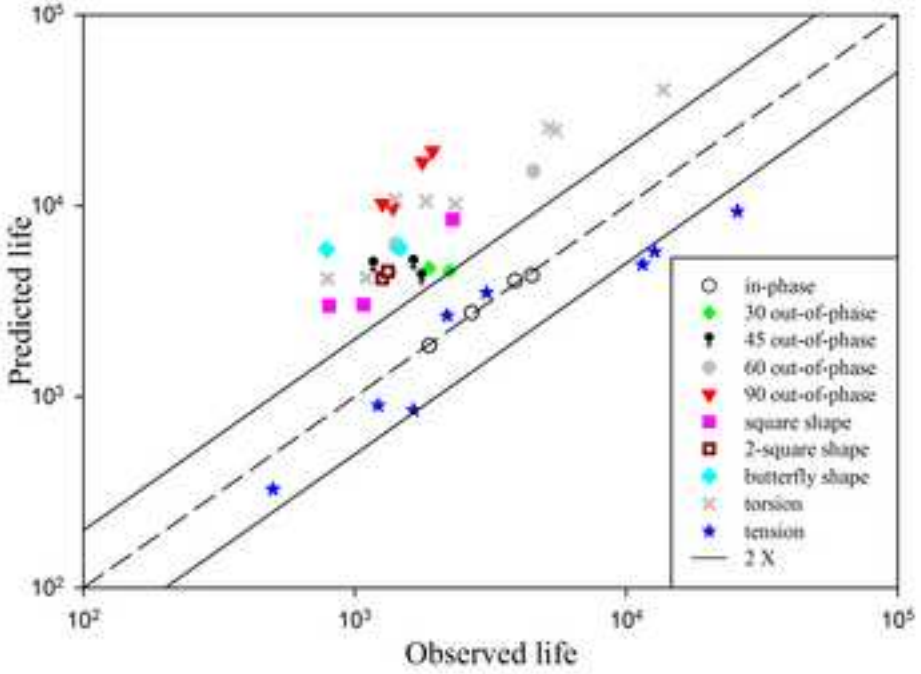

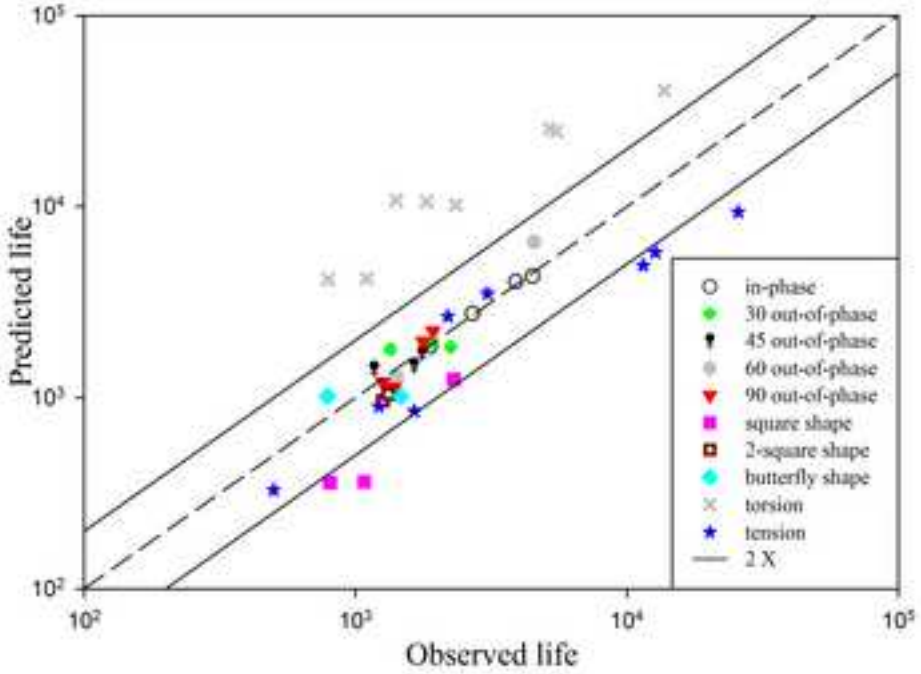

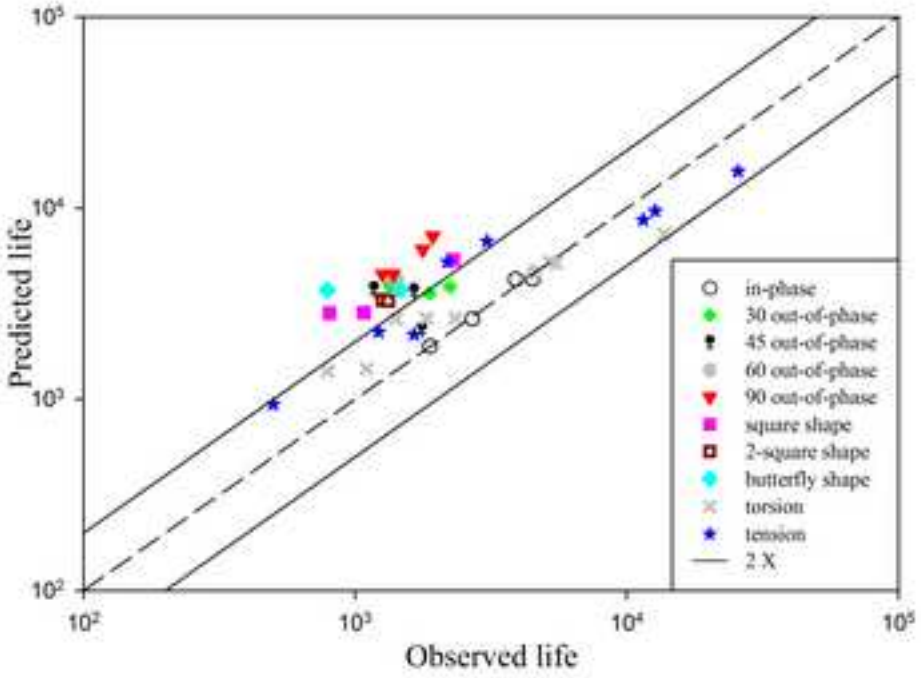

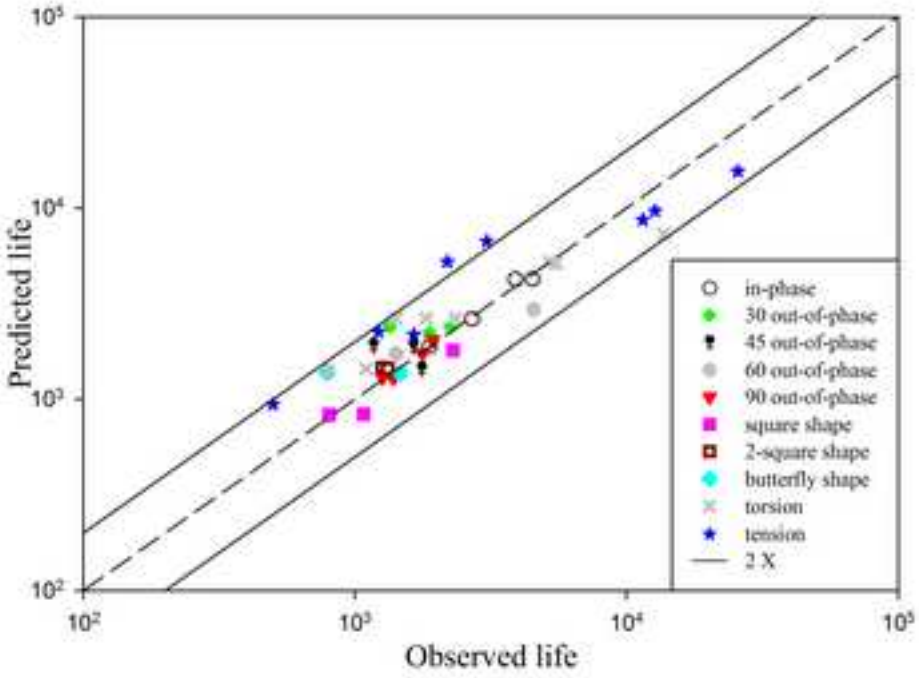

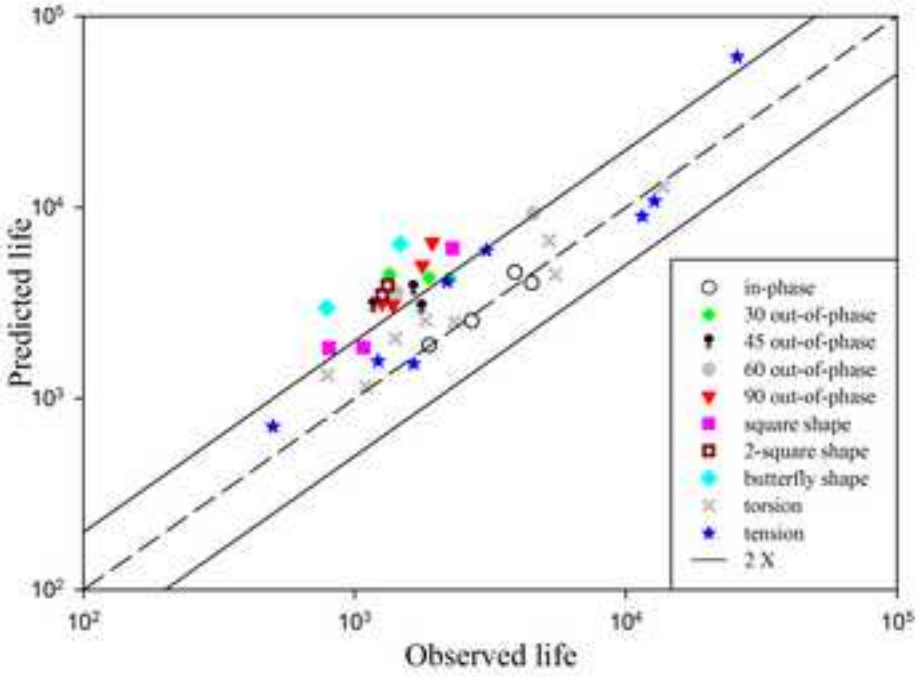

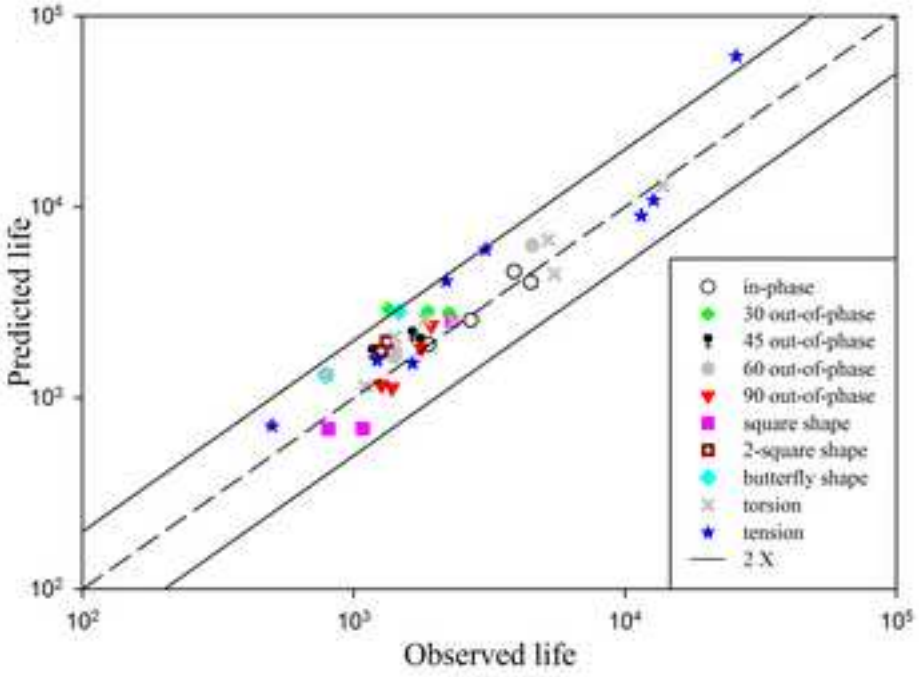

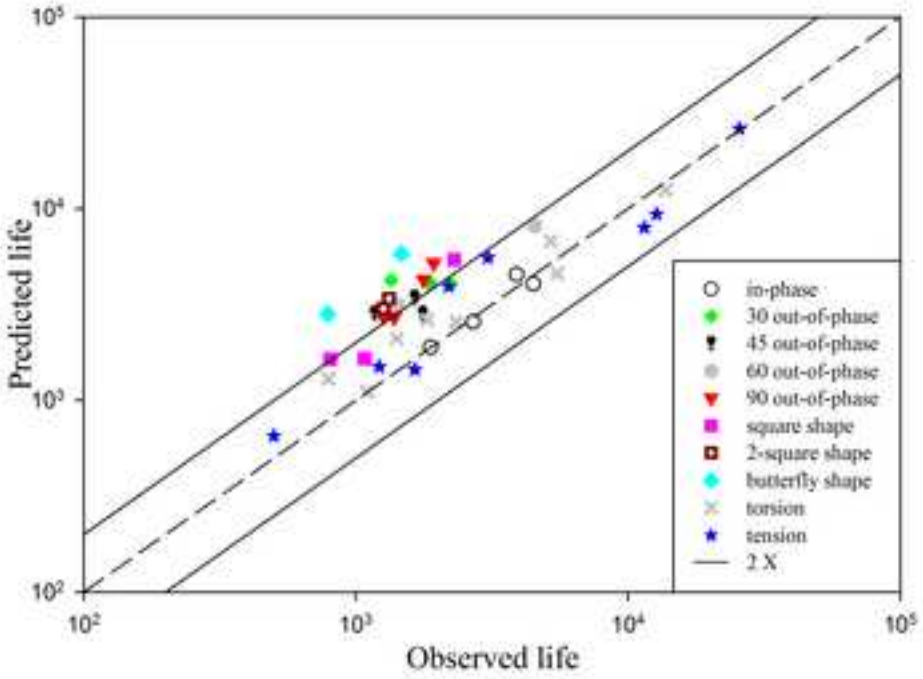

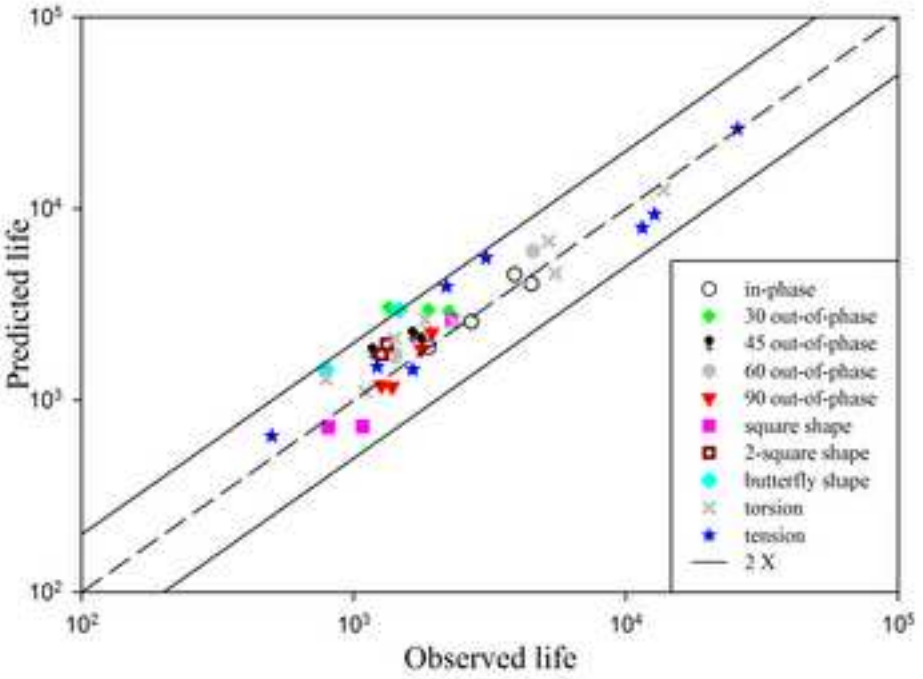

a) 30° out-of-phase (ε_a = 0.0035 , γ_a = 0.0066)

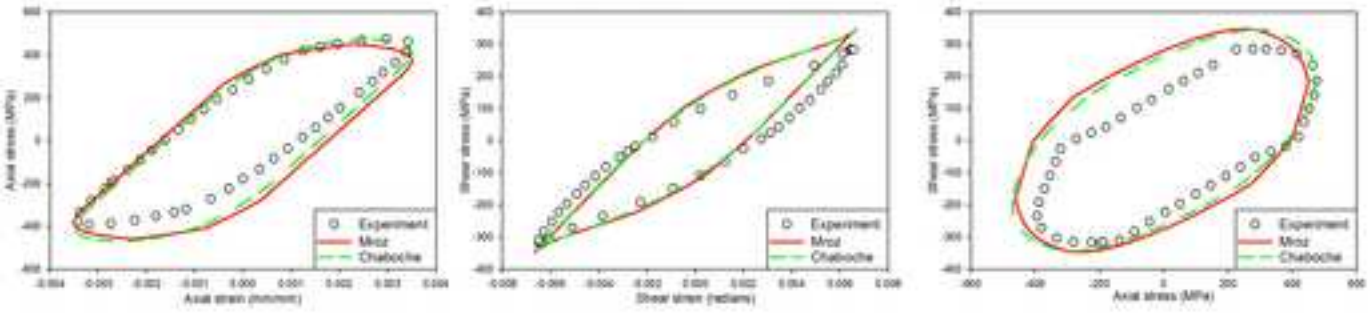

b) 45° out-of-phase (ε_a = 0.0035 , γ_a = 0.0066)

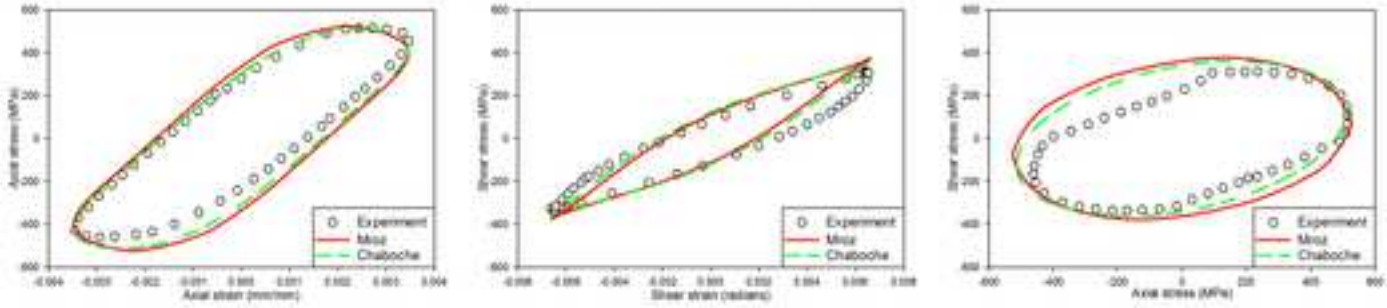

c) 60° out-of-phase (ε_a = 0.0035 , γ_a = 0.0067)

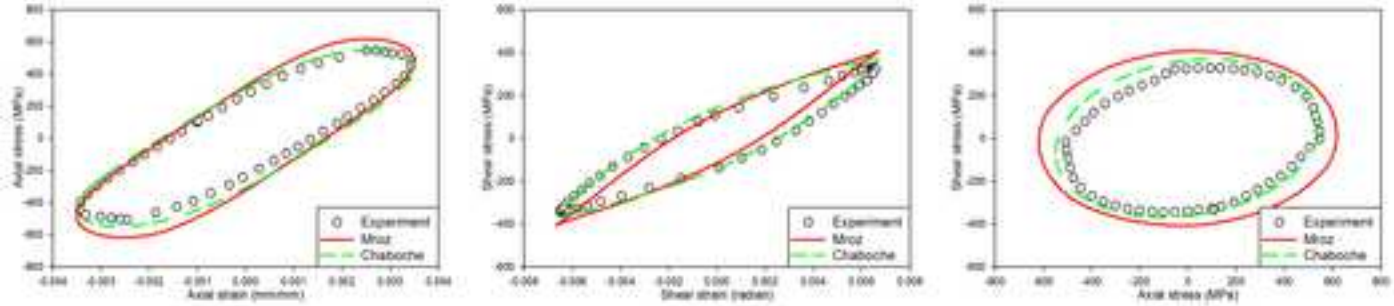

d) 90° out-of-phase (ε_a = 0.0029 , γ_a = 0.0056)

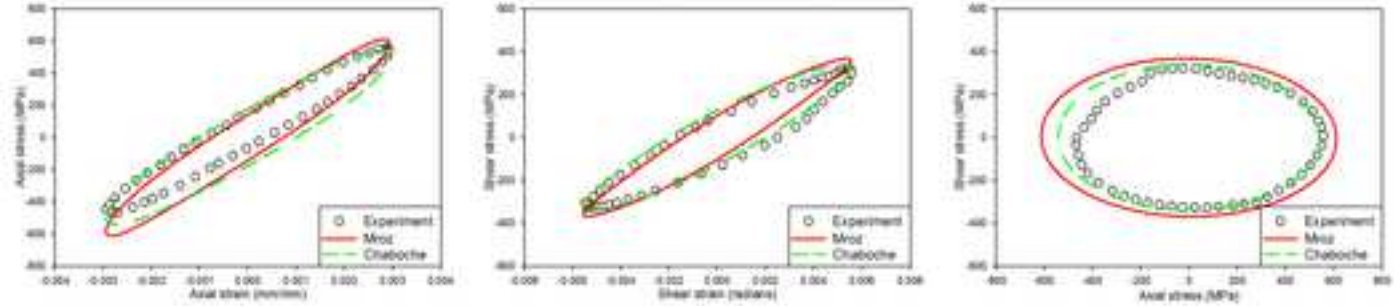

a) Square-shape ($\varepsilon_a = 0.0025$, $\gamma_a = 0.0056$)

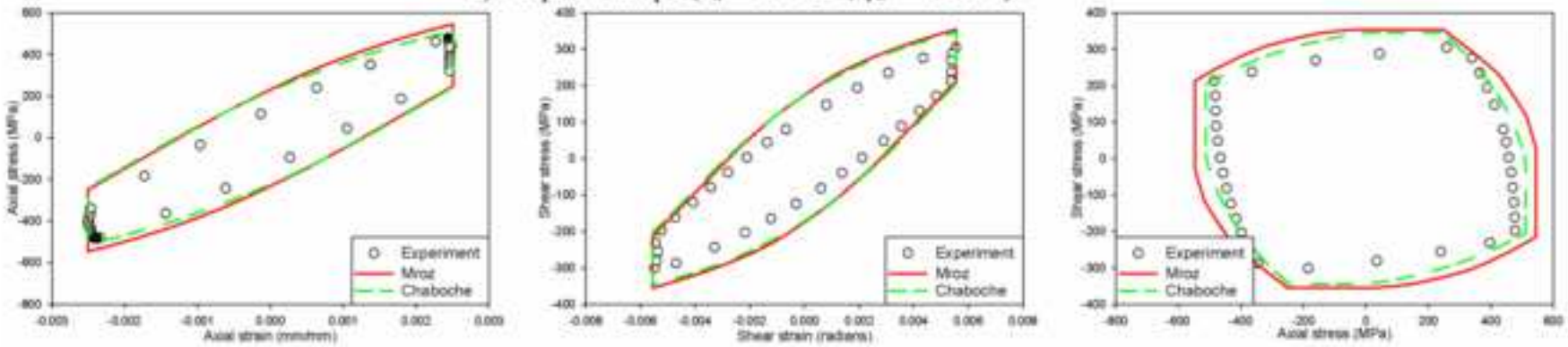

b) Two-square shape ($\varepsilon_a = 0.0035$, $\gamma_a = 0.0038$)

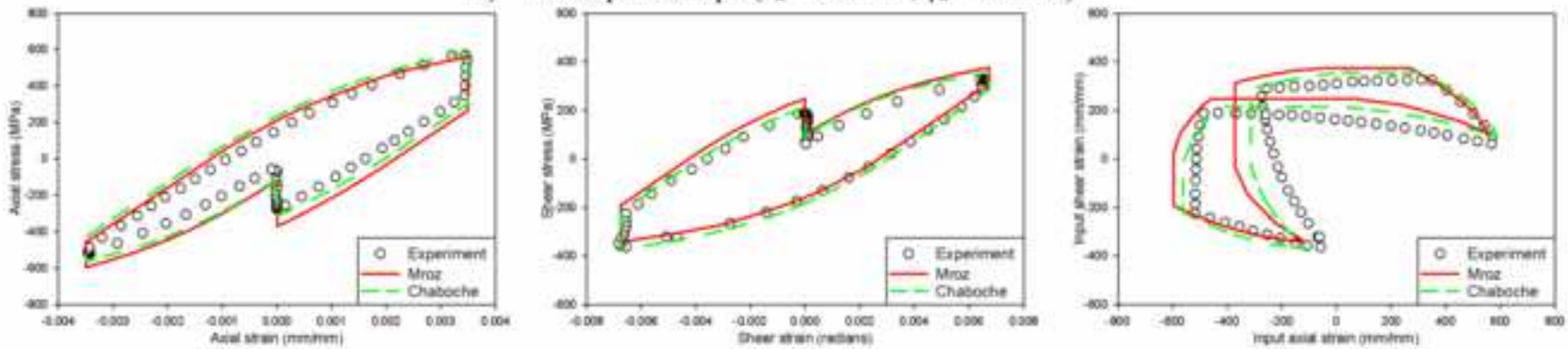

c) Butterfly shape ($\varepsilon_a = 0.0035$, $\gamma_a = 0.0066$)

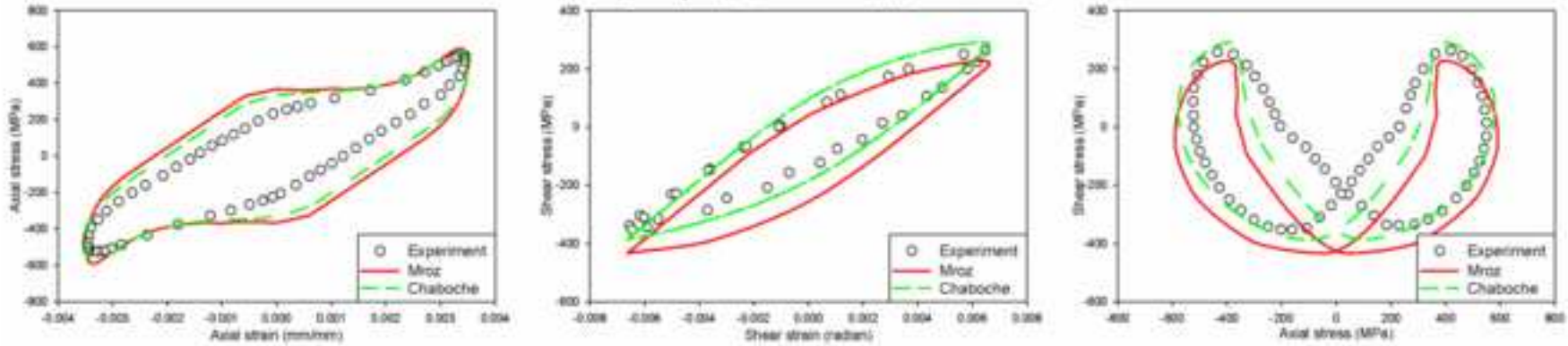

JIJF 2755: Load Path Sensitivity and Fatigue Life Estimation of 30CrNiMo8HH

Research highlights

- New experimental results for multiaxial behaviour of 30CrNiMo8HH steel
- Life reduction of up to five times due to the nonproportionality of load
- A novel material dependent nonproportionality factor is proposed
- Life predictions based on the novel factor falls into a 2x scatter band of the experimental life